Liquid-phase sintering of Ti(C,N)-based cermets. The effects of binder nature and content on the solubility and wettability of hard ceramic phases

By José M. Córdoba*, Ernesto Chicardi and Francisco J. Gotor

(josem.cordoba@csic.es, ernesto.chicardi@icmse.csic.es, fgotor@cica.es)

Instituto de Ciencia de Materiales de Sevilla, Centro Mixto CSIC-US, Américo Vespucio 49, 41092 Sevilla, Spain.

Abstract

Different commercial TiC-TiN/Co/Ni mixtures were used as raw materials for Ti(C,N) cermets, and the effects of the sintering parameters (binder content, binder nature, sintering time and additives) on the final hard ceramic phase were studied at the sintering temperature of 1400 ºC. When Co is used as the binder medium, it is possible to completely convert the starting commercial TiC-TiN mixture into TiC_xN_{1-x}. When Ni is used, which exhibits lower solubilising capacity than Co, the total conversion can never be reached and the metallurgical reactions between TiC and TiN during the liquid-phase sintering are more dependent on the sintering time than on the binder content. However, the use of Co-Ni mixtures, showing a synergic effect between the wettability capacity of Ni and the solubilising capacity of Co, enhances the metallurgical reactions at short sintering times.

Keywords: cermets, carbonitrides, sintering, cobalt, titanium, solid-state reaction

*Corresponding Author. E-mail: josem.cordoba@csic.es Phone: +34 630308357 909218

Introduction

Hard materials are powdered metallurgical products manufactured by liquid-phase sintering, which represents an industrial process of considerable importance because it largely determines the microstructure of the material and its final properties. This process involves sintering a compact that consists of a mixture of different ceramic and metal powders with the aid of a liquid binder phase that forms at temperatures below the melting point of hard ceramic phases [1]. For liquid-phase sintering to be practical, the major ceramic phase should be at least slightly soluble in the liquid phase to enhance liquid atomic diffusion and mass transport, which results in rapid sintering of the components.

At melting, the liquid phase wets and infiltrates the solid grain structure by a combination of reaction and capillary forces. The wetting by capillary attraction also provides a smooth rearrangement of the solid particles and a densification without the need of external pressure. In areas where capillary pressures are high, the ceramic particles tend to dissolve and grow by Ostwald ripening, which is often accompanied by coalescence processes. The driving force for liquid-phase sintering is not only the reduction of surface energy by capillary forces but also the reduction of chemical potential through the dissolution of the original phases and the growth of equilibrium solid phases.

The sintering of hard materials is actually a complex process with complicated metallurgical reactions because they involve different raw-material powders [2]. This difference leads to a fine and stable microstructure that exhibits the typical core/rim

structure, where the cores are partially dissolved raw-material particles on which the rim structure has grown through a dissolution–precipitation process [3-5]. The main disadvantages of liquid-phase sintering relate to the parameters that control the sintering process, the solubility, the diffusivity and the surface energies of the phases present, which, coupled with the rapid rates of sintering, result in less predictability of the final structure and properties.

In this context, the industry is still lacking in understanding the mechanism of liquid-phase sintering of nitrogen-containing cemented carbides. The present work details a systematic approach to fill in these gaps. To understand the behaviour during the sintering of hard materials, the changes that occur in the nature and content of phases were studied as a function of the raw materials, the secondary phases, the content of the binder and the sintering time. The effect on the solubility and wettability of the hard ceramic phase is described.

Materials and Methods

TiC powder (99% purity, Strem Chemicals), TiN powder (99% purity, Strem Chemicals), WC powder (99.5% purity, <1 µm, Strem Chemicals), Mo_2C powder (99.5% purity, Strem Chemicals), Ni powder (puriss., Fluka), Co powder (99.9% purity, <100 mesh, Sigma), Ar gas ($H_2O \leq 8$ ppm and $O_2 \leq 2$ ppm, Linde) and N_2 gas (H_2O and $O_2 \leq 3$ ppm, Air Liquide) were used in the present study.

Commercial TiC+TiN powder mixtures were combined with the binder phase and different additives in the appropriate proportions (see Table I) by hand grinding in an

agate mortar. The mixtures were subsequently sonicated for 10 min in ethanol and dried in an oven at 80 ºC overnight.

Compact bodies were fabricated through a pressureless process. Powdered cermets were first shaped (green bodies) by being isostatically cold pressed at 200 MPa for 5 min to yield cylinders with a diameter of 12 mm and a height of 20 mm. The green bodies were then sintered at 1400 ºC for 0 (**a**), 60 (**b**), 120 (**c)** or 360 (**d**) min (heating rate 10 ºC/min, free cooling) under a flowing Ar atmosphere in a horizontal furnace (type IGM1360 model no. RTH-180-50-1H, AGNI).

X-ray diffraction patterns were obtained with a Panalytical X'Pert Pro instrument equipped with a Θ/Θ goniometer, a Cu K_α radiation source (40 kV, 40 mA), a secondary K_β filter and an X'Celerator detector. The diffraction patterns were scanned from 20º to 80º (2Θ) in step-scan mode at a step of 0.05º and at a counting time of 300 s/step. The TiC_xN_{1-x} lattice parameter (***a***) was calculated from the entire set of peaks in the XRD diagrams from Rietveld analysis using the Fullprof software package and assuming cubic symmetry [6]. The TiC_xN_{1-x} composition was estimated using Vegard's law based on the following reference data file patterns: TiN (38-1420), $TiC_{0.3}N_{0.7}$ (42-1488), $TiC_{0.7}N_{0.3}$ (42-14889) and TiC (32-1383).

Results and Discussion

Figure 1 shows some characteristic X-ray diffraction diagrams of cermets as a function of the sintering time and the nature and content of the binder. The formation during the liquid-phase sintering of a new phase identified as TiC_xN_{1-x} was observed

irrespective of the type of binder employed. For these samples, Table II shows the extent of conversion of TiC and TiN into TiC_xN_{1-x} calculated from the phase quantification obtained by Rietveld analysis of the XRD diagrams. These data are plotted in figure 2, which clearly shows that the evolution of the conversion was strongly dependent not only on the sintering time and the binder content but also on the nature of the binder.

For all the samples, the data in figure 2 could be fitted to exponential equations that showed asymptotic trends, as described by the following general equation:

$$\boldsymbol{\alpha} = A - B\, e^{(-C\mathbf{t})}$$

where $\boldsymbol{\alpha}$ is the extent of conversion, which varies from 0 to 1 as the process progresses from initiation to completion, $\boldsymbol{t}$ is the sintering time (min) and *A*, *B* and *C* are constants (Table III) with the following physical meanings:

- Parameter *A* is related to the TiC_xN_{1-x} conversion attained at the sintering temperature when the sintering time approaches infinity. Values of *A* less than 1 mean that full conversion will never be reached and that the *A* value corresponds to the maximum possible conversion. Values of *A* greater than 1 mean that full conversion can be attained for finite sintering times.
- Parameter *B* accounts for the conversion attained during the heating ramp step until the final sintering temperature is reached.
- Parameter *C* is connected to the conversion rate constant. Higher *C* values result in higher conversion rates.

The calculated exponential fitted profiles (see Table III) show that the liquid-phase sintering at 1400 ºC can completely transform the TiN/TiC mixture into TiC_xN_{1-x} when Co or a mixture of Ni/Co is used as the binder. Furthermore, from the set of

equations shown in Table III, the minimum amount of binder required to achieve complete conversion was estimated. When Co is used as binder, at least 24 wt.% of this element is necessary to completely convert the starting TiC and TiN mixture into TiC_xN_{1-x}. If the binder is a mixture of Co and Ni, a minimum binder content of 36 wt.% is necessary.

If full conversion is possible, the time required to achieve it can also be estimated. For example, sintering times of 567 min and 311 min are necessary when 30 wt.% and 40 wt.% of Co are used as the binder, respectively. When 40 wt.% of a Ni-Co mixture is used, 514 min of sintering time is required for full conversion. Notably, the data in Table III suggest that, in the case of Ni, a total conversion can never be reached even when extremely high Ni contents are used. The conversion is not significantly improved with increasing Ni content; it only increases from 0.53 to 0.66 after being sintered for 360 min when the Ni content is increased from 10 wt.% to 40 wt.%.

The differences observed with respect to the nature of the binder are highlighted in figure 3, which shows the gain in the TiC_xN_{1-x} conversion when the binder content was increased for each binder phase and for each sintering time. This figure illustrates the solubilising capacity of different binders and shows that this capacity improves (slope of the arrows) from pure Ni to pure Co. These differences arise because of the different behaviour with respect to the solubility and wettability of the raw materials in the molten binder. Taking into account that the dissolution of nitrogen is negligible, the key solubility factor is determined by the dissolution of carbon. At 1400 ºC, the solubility of carbon in cobalt is 7 at.% and is 2.7 at.% in nickel **[7]**. Additionally, the surface energy, which determines the wetting behaviour, is slightly higher in cobalt than in nickel (2522-

2550 mJ/m^2 and 2380-2450 mJ/m^2, respectively) **[**8-9**]**. A higher surface energy results in greater cohesive forces of the liquid metal drops and hence leads to higher contact angles, which reduces the wettability.

For a 10 wt.% binder content, the effect of the greater wettability of Ni balanced the greater solubility of Co, and similar conversion values were found (figures 2(a) and 2(d) and Table II), independent of the sintering time. However, when the binder content was increased, the solubility effect became predominant when the sintering time was prolonged. Although the conversion at 0 min for Ni and Co was similar independent of the binder content, the differences between Co and Ni were ever greater when the binder content and sintering time were increased, and full conversion was reached only when Co was used (figure 2 and Table II).

The significant behaviour observed for the Co-Ni mixture, where the conversion at 0 min increased considerably with increasing binder content (figure 2(c)), is notable. This behaviour reflects the synergy between the capabilities of wettability and solubility of Ni and Co, respectively. This synergic effect was lost with prolonged sintering times because the final conversion in these cases is determined mainly by the ability of the binder to solubilise the ceramic particles. The presence of a smaller amount of Co in comparison with samples that contained pure Co reduced the solubility capacity of the Co-Ni mixture, and the conversion rate was decreased.

The data in figure 2(b) and Table II show that the presence of WC or Mo_2C as an additive slowed the conversion of TiC and TiN into TiC_xN_{1-x} compared with that of samples without additives. The WC and Mo_2C exhibit high solubility values in Co (39 wt% at 1400 ºC for both phases) [10], and they were observed to dissolve in the binder at

temperatures less than 1200 ºC —well before any liquid is formed (the eutectic temperature is ~1320 ºC) **[**11**]**. The dissolution of the additive phases in the binder was corroborated by the XRD profiles shown in figure 4 (samples **R**2CoWCc and **R**2CoMo$_2$Cc), where WC and Mo$_2$C were not observed. In sample **R**2WCc, free W was detected, which demonstrated that dissolution occurred through decomposition because its elemental constituents incorporated into the binder. The presence of carbon in the melted binder due to the dissolution of the additive phases induced a lower TiC solubility, and therefore a lower conversion into TiC_xN_{1-x}.

The lattice parameter of the TiC_xN_{1-x} phase calculated from the XRD measurements ranged from 4.2812 Å to 4.2905 Å. The composition was determined under the assumption that the behaviour was consistent with Vegard's law, and *x* values between 0.48 and 0.64 were observed (see Table IV). Although the compositional range observed for all the samples was narrow, some trends were observed. The TiC_xN_{1-x} phase formed when Co was used contained lower C contents than that formed with pure Ni, most likely because of the greater capacity of cobalt to dissolve carbon. The use of a Co-Ni mixture as the binder further reduced the compositional range of TiC_xN_{1-x}, and a practically constant composition was observed. Similar values were observed when additives were employed. A slightly higher carbon content in the final titanium carbonitride was noticed, which was due to the carbon contribution of the additive carbide phases.

Conclusions

The research performed during this study provides a simple way to obtain a model for high-temperature metallurgical reactions between commercial TiC and TiN within a liquid-phase solvent medium (cobalt and/or nickel at 1400 ºC). We have attempted to provide an indication of the roles of wettability and solubility during liquid-phase sintering. The greater solubilising capacity of Co when it is used as the binder medium enhances the metallurgical reactions between TiC and TiN; their extension increases with time and predominantly with the binder content. When Ni is used, which exhibits a lower solubilising capacity, the extent of the metallurgical reactions is reduced, and the reactions are more dependent on the sintering time than on the binder content. However, because the Ni has greater wettability capacity than Co, the differences between the two binders are not as pronounced for short sintering times and low binder contents. Furthermore, the synergic effect between the wettability capacity of Ni and the solubilising capacity of Co allows the Co-Ni mixtures to accelerate the metallurgical reactions at short sintering times when the binder content is increased. Nevertheless, when the sintering is prolonged, the extension of the metallurgical reactions is mainly determined by the Co content in the binder mixture.

Acknowledgments

This work was supported by the Spanish government under grant No. MAT2011-22981, which is financed in part by the European Regional Development Fund of 2007-2013. E. Chicardi and J. M. Córdoba were supported by CSIC through JAE-Pre and JAE-Doc grants, respectively, which are financed in part by the European Social Fund (ESF).

References

[1] R. M. German, P. Suri, S. J. Park, Review: Liquid phase sintering, J. Mater. Sci., 44 (2009) 1–39

[2] P. Wally', S. Binder, P. Ettmayer, W. Lengauer, Reaction of compact carbonitrides with liquid binder metals, J. All. Comps., 230 (1995) 53-57

[3] H.O. Andrén, Microstructures of cemented carbides, Mater. Design, 22 (2001) 491-498

[4] S.Y. Ahn, S.W. Kim, S. Kang, Microstructure of Ti(C,N)-WC-NbC-Ni cermets, J. Am. Ceram. Soc., 84[4] (2001) 846-849

[5] S.Y. Ahn, S. Kang, Formation of core7rim structures in Ti(C,N)-WC-Ni cermets via dissolution and precipitation process, J. Am. Ceram. Soc., 83 [6] (200) 1489-1494

[6] J. Rodríguez-Carvajal and R. Thiery, FullProf ILL May-2010.

[7] F.R. de Boer, R. Boom, W.C.M.Mattens, A.R. Miedema, A.K. Niessen, Cohesion in Metals, North Holland, Amsterdam, 1988.

[8] ASM Handbook, volume 3, Alloy Phase Diagrams, ASM International, ed. The Materials Information Company, 1992, USA.

[9] W.R. Tyson, W.A. Miller, Surface free energies of solid metals: estimation from liquid surface tension measurements, Surf. Sci. 62 (1977) 267.

[10] R. Kieffer, P. Ettmayer, M. Freudhofmeier, About nitrides and carbonitrides and nitrides based cemented hard alloys, Modern Develop. Powder Metal., ed. by H. Hausner, vol. 5 (1971) 201-204

[11] H.O. Andrén, U. Rolander, P. Lindahl, Phase composition in cemented carbides and cermets, Int. J. Refract. Metals Hard. Mater. 12 (1993-1994) 107-113.

Figure Captions

Figure 1. Characteristics XRD diagrams of cermets that allow a comparison of different sintering times, binder contents and binder natures. (***1***; TiC, ***2***; TiN and ***3***; TiC_xN_{1-x})

Figure 2. TiC_xN_{1-x} conversion for cermets as a function of the sintering time using (□) 10 wt.%, (Δ) 20 wt.%, (★) 30 wt.% or (◊) 40 wt% binder: (a) Co, (b) 20 wt.% Co with 5 wt.% additives (Δ, no additives; ○**,** WC; ✯, Mo_2C), (c) a mixture of Ni and Co and (d) Ni.

Figure 3. $\alpha_{x\%}$-$\alpha_{x\%-10}$ versus sintering time for every set of cermets. Solubility capacities are marked by arrows (Co>Co-Ni>Ni).

Figure 4. Characteristics XRD profiles of type **R2**-Co cermets with additives (sintering time 120 min). (***1***; TiC, ***2***; TiN and ***3***; TiC_xN_{1-x})

Table I. Raw-material contents (wt.%) and labels for the different cermets studied.

Sample			Initial Composition
R1Co	**R**1CoNi	**R**1Ni	45%TiC+45%TiN+10% X
R2Co	**R**2CoNi	**R**2Ni	40%TiC+40%TiN+20% X
R3Co	**R**3CoNi	**R**3Ni	35%TiC+35%TiN+30% X
R4Co	**R**4CoNi	**R**4Ni	30%TiC+30%TiN+40% X
R2CoWC			37.5%TiC+37.5%TiN+20%Co+5%WC
R2CoMo$_2$C			37.5%TiC+37.5%TiN+20%Co+5%Mo$_2$C

X: Cobalt, nickel or cobalt-nickel mixture (50-50 wt.%)

Table II. Extent of TiC_xN_{1-x}conversion, **α**, after the liquid-phase sintering at 1400 ºC of the cermets listed in Table I. (* full conversion was reached). Sintering time: (**a**) 0 min, (**b**) 60 min, (**c)** 120 min and (**d**) 360 min.

Samples without additives					
Sample	**α**	**Sample**	**α**	**Sample**	**α**
R1Coa	0.10	**R**1CoNia	0.06	**R**1Nia	0.08
R1Cob	0.21	**R**1CoNib	0.13	**R**1Nib	0.22
R1Coc	0.31	**R**1CoNic	0.19	**R**1Nic	0.30
R1Cod	0.54	**R**1CoNid	0.36	**R**1Nid	0.53
R2Coa	0.13	**R**2CoNia	0.13	**R**2Nia	0.09
R2Cob	0.26	**R**2CoNib	0.24	**R**2Nib	0.24
R2Coc	0.40	**R**2CoNic	0.33	**R**2Nic	0.33
R2Cod	0.68	**R**2CoNid	0.55	**R**2Nid	0.58
R3Coa	0.16	**R**3CoNia	0.25	**R**3Nia	0.11
R3Cob	0.35	**R**3CoNib	0.38	**R**3Nib	0.28
R3Coc	0.51	**R**3CoNic	0.48	**R**3Nic	0.38
R3Cod	0.87	**R**3CoNid	0.72	**R**3Nid	0.63
R4Coa	0.19	**R**4CoNia	0.42	**R**4Nia	0.14
R4Cob	0.44	**R**4CoNib	0.57	**R**4Nib	0.30
R4Coc	0.69	**R**4CoNic	0.68	**R**4Nic	0.42
R4Cod	1.00*	**R**4CoNid	0.93	**R**4Nid	0.66
Samples with additives					
Sample	**α**		**Sample**	**α**	
R2CoWCa	0.07		**R**2CoMo$_2$Ca	0.08	
R2CoWCb	0.20		**R**2CoMo$_2$Cb	0.20	
R2CoWCc	0.25		**R**2CoMo$_2$Cc	0.27	
R2COWCd	0.42		**R**2CoMo$_2$Cd	0.44	

Table III. Equation coefficients that define the TiC_xN_{1-x} conversion (**α**) as a function of the sintering time for the different samples studied [**α** = A - B $e^{(-t/C)}$] (* A is a theoretical data obtained from the extrapolation of the other values).

Sample	A	B	C	Adj. R- Square
R1Co	0.76	0.66	3.09E-03	0.989
R2Co	0.91	0.79	3.45E-03	0.998
R3Co	1.11	0.95	3.83E-03	0.996
R4Co(*)	1.28	1.09	4.38E-03	0.987
R1CoNi	0.53	0.47	2.78E-03	0.994
R2CoNi	0.72	0.58	3.47E-03	0.991
R3CoNi	0.87	0.61	3.92E-03	0.986
R4CoNi	1.07	0.64	4.31E-03	0.994
R1Ni	0.66	0.58	4.03E-03	0.991
R2Ni	0.71	0.61	4.25E-03	0.989
R3Ni	0.74	0.63	4.66E-03	0.985
R4Ni	0.77	0.64	4.76E-03	0.993
R2CoWC	0.52	0.44	4.83E-03	0.996
R2CoMo$_2$C	0.49	0.41	4.96E-03	0.989

Table IV. Summary of the TiC_xN_{1-x} stoichiometry, ***x***, in the cermets with and without additives determined assuming Vegard's law. Sintering time: (**a**) 0 min, (**b**) 60 min, (**c**) 120 min and (**d**) 360 min.

Samples without additives					
Sample	***x***	**Sample**	***x***	**Sample**	***x***
R1Coa	0.52	**R**1CoNia	0.53	**R**1Nia	0.56
R1Cob	0.53	**R**1CoNib	0.52	**R**1Nib	0.59
R1Coc	0.57	**R**1CoNic	0.48	**R**1Nic	0.55
R1Cod	0.56	**R**1CoNid	0.50	**R**1Nid	0.60
R2Coa	0.59	**R**2CoNia	0.52	**R**2Nia	0.61
R2Cob	0.56	**R**2CoNib	0.48	**R**2Nib	0.64
R2Coc	0.53	**R**2CoNic	0.53	**R**2Nic	0.62
R2Cod	0.49	**R**2CoNid	0.52	**R**2Nid	0.56
R3Coa	0.53	**R**3CoNia	0.54	**R**3Nia	0.56
R3Cob	0.53	**R**3CoNib	0.50	**R**3Nib	0.63
R3Coc	0.51	**R**3CoNic	0.49	**R**3Nic	0.64
R3Cod	0.49	**R**3CoNid	0.53	**R**3Nid	0.53
R4Coa	0.55	**R**4CoNia	0.50	**R**4Nia	0.56
R4Cob	0.59	**R**4CoNib	0.49	**R**4Nib	0.60
R4Coc	0.54	**R**4CoNic	0.48	**R**4Nic	0.54
R4Cod	0.52	**R**4CoNid	0.51	**R**4Nid	0.53
Samples with additives					
Sample	**TiC_xN_{1-x}**		**Sample**	**TiC_xN_{1-x}**	
R2CoWCa	0.51		**R**2CoMo$_2$Ca	0.66	
R2CoWCb	0.59		**R**2CoMo$_2$Cb	0.68	
R2CoWCc	0.56		**R**2CoMo$_2$Cc	0.69	
R2COWCd	0.57		**R**2CoMo$_2$Cd	0.51	

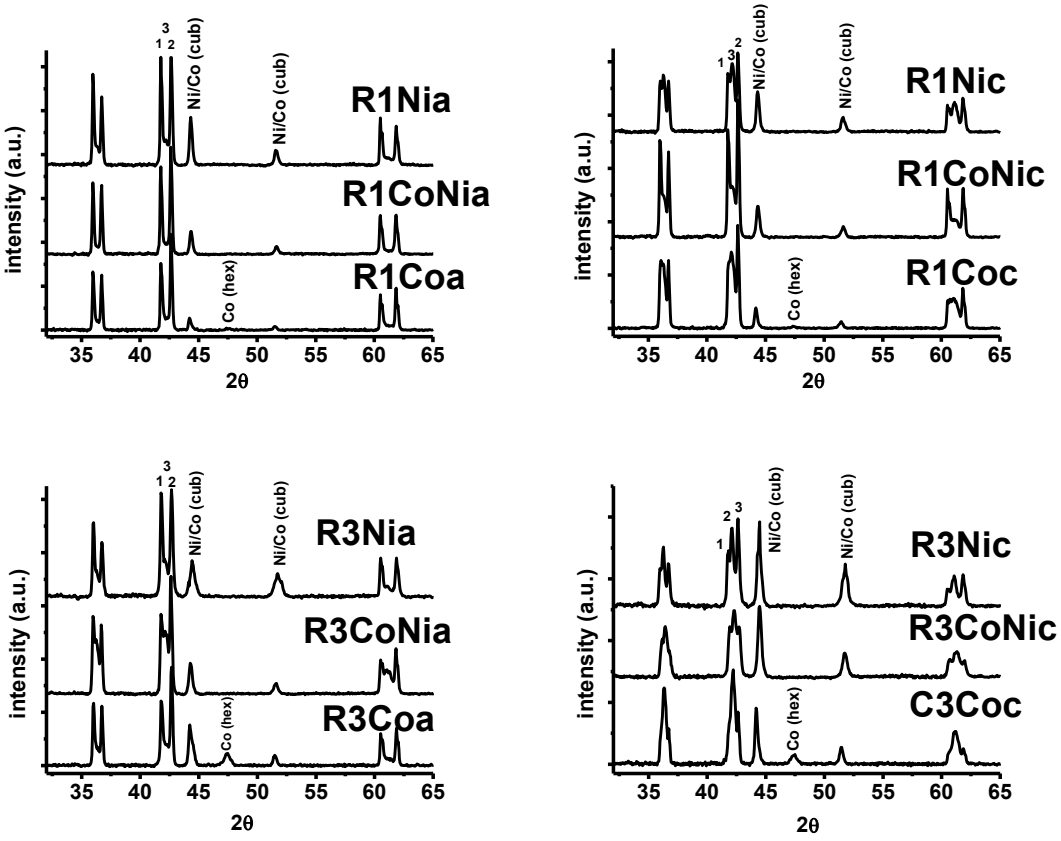
R1Nia
R1CoNia
R1Coa
R1Nic
R1CoNic
R1Coc
R3Nia
R3CoNia
R3Coa
R3Nic
R3CoNic
C3Coc
Ni/Co (cub)
Co (hex)
intensity (a.u.)
2θ
35
40
45
50
55
60
65

Figure 1

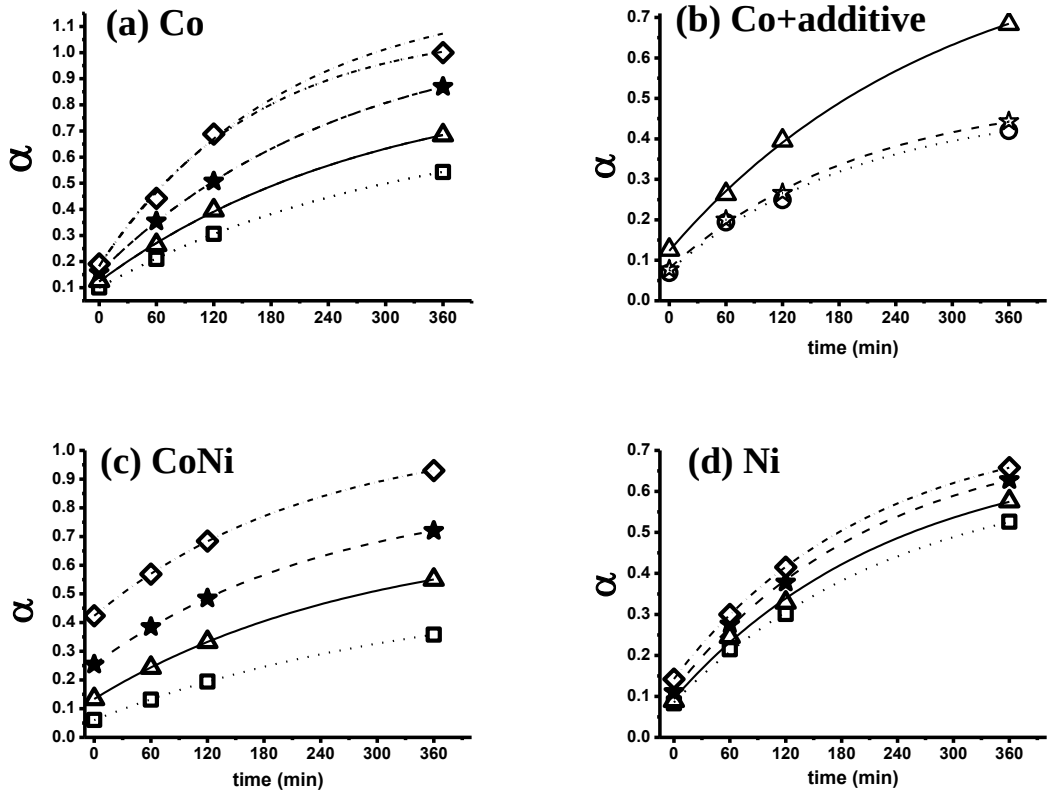

Figure 2

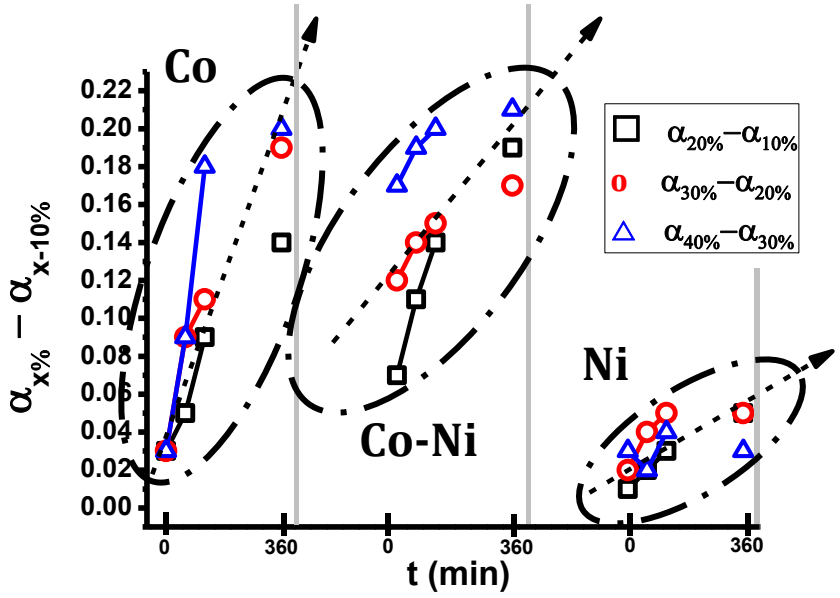
Co
Co-Ni
Ni
$\alpha_{20\%}-\alpha_{10\%}$
$\alpha_{30\%}-\alpha_{20\%}$
$\alpha_{40\%}-\alpha_{30\%}$
$\alpha_{x\%} - \alpha_{x-10\%}$
t (min)
0.22
0.20
0.18
0.16
0.14
0.12
0.10
0.08
0.06
0.04
0.02
0.00
0
360
0
360
0
360

Figure 3

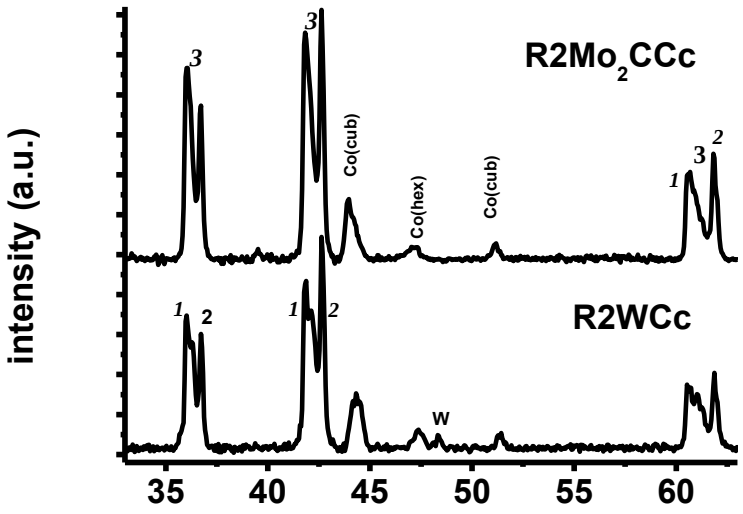
intensity (a.u.)
R2Mo2CCc
R2WCc
Co(cub)
Co(hex)
Co(cub)
W
1
2
3
35
40
45
50
55
60

Figure 4